# THE STRUCTURE OF THE VELOCITY FIELD IN AN EXPERIMENTAL FORCED BOX TURBULENCE

**J.F. Krawczynski, B. Renou, L. Danaila**
CORIA UMR 6614,
University of Rouen
Avenue de l'Université BP12, 76821 Saint Etiene du Rouvray, France
renou@coria.fr

**P.E. Dimotakis**
Graduate Aeronautical Laboratories, California Institute of Technology
Pasadena, California, U.S.A.
dimotakis@caltech.edu

## ABSTRACT

We document an experimental investigation of a reactor in which fluid is injected through two sets of 16 opposed jets that issue from top/bottom boundary porous planes. The resulting confined flow produces pairs of opposed counter-current annular mixing layers. The mean velocity field and statistical properties of the turbulent flow are investigated. The velocity spectrum, inferred from planar PIV (Particle Image Velocimetry), presents a scaling-range region that behaves as $k^{-3}$ over a relatively wide range of scales. The spectral behavior is interpreted in terms of stagnation-point flows and counter-current mixing layers, that drive the confined flow.

## INTRODUCTION

The motivation for the work, of which this contribution is a part, is to improve the understanding of turbulent mixing for a wide spectrum of applications, including combustion, propulsion, chemical-process, and other industrial problems. The flow in many of these applications is confined and it is important to investigate the effects that confinement has on the turbulence, especially since much of the theory and modeling is often based on experience derived from unconfined turbulent flows. Sometimes, the aim in these applications is 'imperfect mixing', in which fluctuations are desired. Predicting the mixing extent, as opposed to striving to increase it, is also part of the goal. The fundamental characterization and the ability to predict the behavior of confined turbulent flows and the mixing that ensues are important.

Traditional methods for achieving good mixing often employ closed vessels or reactors where the turbulence is confined. From a fundamental viewpoint, such a reactor can be viewed as a forced, box turbulence (FBT). Flows in such reactors have been studied, for example, by Birouk et al. (2003), Hwang and Eaton (2003), and Krawczynski et al. (2006a) who investigated both velocity- and scalar-field behavior. Propellers or HEV (High Efficiency Vortex) are also common techniques aimed at better mixing. Interest in such forced turbulence is motivated by fundamental questions on turbulence, practical applications, testing micromixing and SGS (subgrid-scale) models, evaluating new experimental methods, etc. Testing complex issues under controlled, laboratory conditions, over a wide range of Reynolds numbers, is also important.

Compared with more-conventional methods to generate homogeneous and isotropic flows, such as grid turbulence, closed-vessel turbulence can generate high-intensity turbulent fluctuations. Birouk et al. (2003) reported nearly stationary, homogeneous, and isotropic (SHI) flow generated in the centre of their nearly spherical interior, using eight variable-speed fans. In this low-mean-flow region, Taylor microscale Reynolds numbers of $Re_\lambda \approx 110$ were achieved.

Hwang and Eaton (2003) used a chamber that was approximately spherical in its interior, with turbulence generated by eight synthetic-jet actuators. It also generated a nearly stationary, homogeneous, and isotropic velocity field in the centre, with very low mean flow velocities. Higher turbulence levels than those reported in Birouk et al. (2003) were achieved, with $Re_\lambda$ up to 218.

Previous work, reported in Krawczynski et al. (2006a), primarily focused on a proper determination of small-scale quantities of scalar mixing. The reactor investigated in those experiments was a cubic box ($64\,\mathrm{cm}^3$) in which fluid was injected through 12 inlets, located on two opposite planes, pointing towards the centre of the reactor. Results inferred from single-point laser measurements showed good global homogeneity and isotropy of the velocity field at large scales. However, the small size of the experiment set-up resulted in relatively small Taylor micro-scale Reynolds numbers ($Re_\lambda \approx 60$).

The flow in such reactors is strongly dependent on inlet conditions. In typical configurations, fluid is injected through jets, for which the main parameters are: the jet-injection Reynolds number, $Re_{\mathrm{inj}}$, and the height scaled by the number of diameters, i.e., $H/D$ with $D$ the diameter of the injecting jets, and $H$ is the reactor mid-height. Most studies of flows with jets have focused on the self-similar region (beyond $15D$), with less attention paid to the injection (near-field) region (closer than $5D$). However, in most combustion applications, jets discharge in small closed chambers and can develop only over relatively short distances. Markides and Mastorakos (2006) studied scalar dispersion in such a flow, paying particular attention to scalar dissipation.

The present paper addresses the experimental characterization of a Forced Box Turbulence (FBT) flow. The basic pattern in the resulting confined flow is a pair of opposed, confined impinging jets. Particular to this flow is that 16 such patterns coexist and interact in the reactor. This leads to local confinement of the basic, periodic pattern. The fluid in this reactor is locally confined and forced to exit through

the top/bottom injection boundary plates, as opposed to the flow that would result from only a pair of opposed jets that would invade the whole volume.

## EXPERIMENTAL SET-UP AND MEASUREMENT SYSTEM

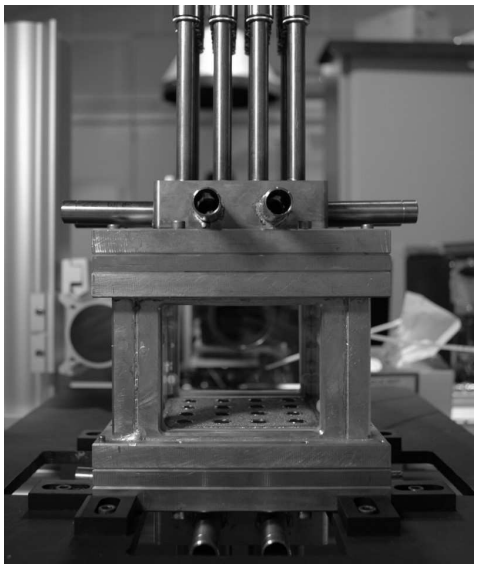

Figure 1: Experimental set-up.

The basic design allows for a modular and flexible experiment, generating flows in which velocity and scalar fields can be simultaneously investigated, over a range of pressures. The reactor interior (Fig. 1) is a rectangular parallelepiped ($110\times110\times60\,\mathrm{mm}^3$) equipped with quartz Suprasil windows ($100\times80\,\mathrm{mm}^2$). The top/bottom porous boundary plates are backed by plena connected to an exhaust piping network through 8 exhaust ports on each cap. Each plenum provides 16 tubes that supply the top/bottom jets individually. Two types of tubes are employed. These are 200 mm long, but with an inner diameter of either $D = 10\,\mathrm{mm}$ or $D = 6\,\mathrm{mm}$, respectively, arranged on a 24 mm-spacing rectangular matrix. Thus, the horizontal distance between two neighboring jet axes is $2\times L = 24\,\mathrm{mm}$.

This is an optimal 16-jet geometry from the point of view of various symmetries. This aligned-jet configuration produces a (mean) stagnation plane in the centre of the reactor, where the mean velocity is (almost) zero everywhere. Injected fluid enters at high-enough $Re_{\mathrm{inj}}$ to be fully turbulent. To document internal conditions, one wall is equipped with a 1 mm-diameter pressure tap, connected to a digital manometer. Micrometric regulating valves are used to match flow rates from each of the jets and between the two opposed discharge plena.

### Velocity field measurements

The experimental conditions are documented in Table 1. Most results are presented for the Reynolds numbers listed.

The ensemble-averaged displacement of oil particles between pairs of images is estimated using a PIV cross-correlation technique. The light source is a Nd-Yag laser (Big Sky laser, 120 mJ/pulse) with a second-harmonic-generating crystal that produces a Q-switched laser output in the green (532 nm). Light scattered from the particles is collected on a CCD camera (FlowMaster La Vision, 12 bits, $1280\times1024\,\mathrm{pix}^2$) with a 50 mm f/1.2 Nikkor lens, yielding a magnification of 20.5 pix/mm. The initial size of the PIV interrogation window is $64\,\mathrm{pix}^2$. Six iterations are used to obtain a final interrogation window size of $16\,\mathrm{pix}^2$, with a 50% overlap.

| Case | | A | B | C |
|---|---|---|---|---|
| Inj. diameter | D [mm] | 10 | 10 | 6 |
| Half-height | $H$ [mm], $H/D$ | 30, 3 | 30, 3 | 30,5 |
| Flow rate | $Q_v$ $[m^3/h]$ | 60 | 155.2 | 155.2 |
| Inj. velocity | $V_{\mathrm{inj}}$ $[m/s]$ | 6.63 | 17.15 | 47.65 |
| Residence time | $\tau_{\mathrm{R}}$ [ms] | 44 | 17 | 17 |
| Pressure | $P$ [bar] | 1. | 1.4 | 1.4 |
| Kinematic visc. | $\nu\,[\mathrm{m}^2/\mathrm{s}]\ \times10^{-5}$ | 1. | 1.097 | 1.097 |
| Reynolds nb. | $Re = V_{\mathrm{inj}}\cdot D/\nu$ | 4540 | 15640 | 26061 |

Table 1: Experimental conditions.

The spatial resolution of the measurements is determined according to the PIV transfer function (Foucault et al. 2004). This analysis yields a size of the field of view of $f_{\max} = 1.10^{-3}$/pix that corresponds to a spatial scale of $\simeq 50\,\mathrm{mm}$ and a cut-off spatial frequency for the PIV system of $f_{\mathrm{c}} = 2.8.10^{-2}$/pix corresponding to a scale of $\simeq 1.75\,\mathrm{mm}$. These spatial resolutions are fixed in a given experimental configuration and do not depend on the flow.

## DESCRIPTION OF THE MEAN FLOW

We describe the flow based on planar cuts, either in the jet-axis plane, or in the mid-span plane (cf. Fig. 2, that illustrates the flow resulting from four pairs of opposed jets).

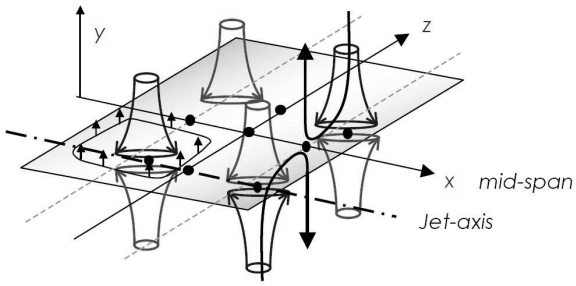


Figure 2: Schematic of the flow.

Arrows in Fig. 2 represent schematic trajectories of particles transported by the mean velocity field only. Particle images are recorded in the $Oxy$-plane (or parallel to it), where $x$ is the horizontal direction and $y$ the vertical axial direction. In the following, $y = 0$ is located on the stagnation plane, while $x = 0$ is located in the middle of the plane of interest.

Figure 3 represents the mean vertical velocity field, $V$, and the mean horizontal velocity field, $U$ (Fig. 4), in the jet-axis plane, normalized by the injection velocity $V_{inj}$, for two pairs of opposed jets. An important feature is the periodicity and symmetry of this flow that are well-captured by the experimental implementation. A mean stagnation region, with a zero-mean axial velocity is created by the impingement of the jets. However, the radial velocity component remains non-negligible in this plane, even though its average value over the plane is zero, as it must be by symmetry.

Two types of stagnation points are located in the stagnation region and are illustrated on these figures. Type-1 stagnation points are produced by the impingement of the opposed jets. (Near-)axisymmetry statistical properties are expected there. Away from these stagnation regions, the

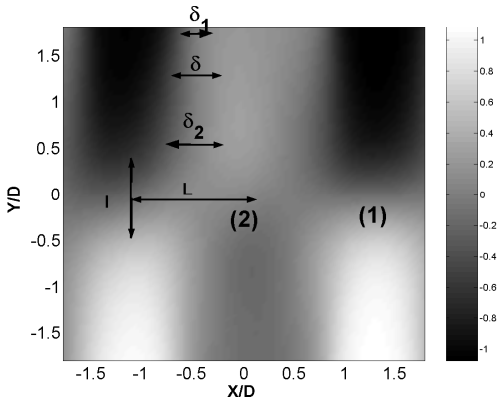


Figure 3: Mean axial velocity field in the jet-axis plane, normalized by the injection velocity $V_{inj}$ (case $B$).

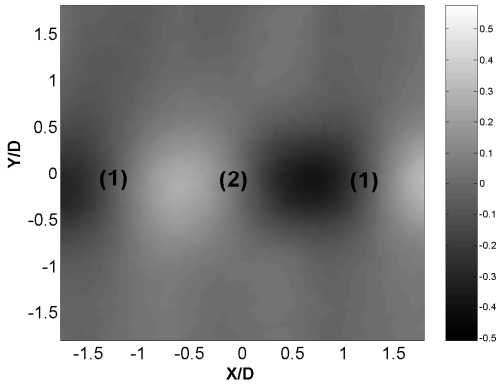


Figure 4: Mean radial velocity field in the jet-axis plane, normalized by the injection velocity, $U/V_{inj}$ (case $B$).

flow turns in the radial direction and the mean radial velocity component, $U$, becomes larger than the axial component, $V$. This region of the reactor can be compared to jets impinging on a flat plate, or turbulent opposed impinging jets, that have been studied before, e.g., Rolon et al. (1991) and Kostiuk et al. (1993).

Type-2 stagnation points occur at the mid-distance between pairs of jets and are not (statistically) axisymmetric. We are not aware of results previously reported for such pairs of opposed jets.

Figure 3 illustrates three characteristic scales of the flow:
a) the scale $\ell$, over which the vertical velocity gradients are steep;
b) the energy injection outer-flow length scale, $L$. This is the distance between the axis of the jet ($x/D = \pm 1.2$) and the mid-distance between jets. Kinetic energy is principally injected in the form of $v$ fluctuations over a scale $\ell$ over which the axial velocity $V$ decreases to zero. Kinetic energy generating $u$ fluctuations is supplied over a scale $L$. The particular design of the reactor allows $\ell \approx D \approx L$, so both $u$ and $v$ fluctuations are energized at the same scales.
c) The vertical mean velocity map highlights another characteristic length scale, $\delta$, the width of the mixing layers. This scale is determined using the same procedure employed to determine the characteristic length of a mixing layer (e.g., Dimotakis 1991, Pope 2000). The scale $\delta$ is basically fixed by the geometrical confinement, and varies between $\delta_1$ (near the injection) and $\delta_2$ (central zone of the reactor), with $\delta_1 < \delta_2$. Note that $\delta$ is only weakly dependent on $y$ in our flow, whereas it grows in free (unconfined) mixing layers, where it evolves with downstream distance.

Obtaining a plane mean stagnation region presents a challenge in the present and similar experiments. Rolon et al. (1991) and Kostiuk et al. (1993) also reported this, for the simpler case of two opposed jets. The level of difficulty is higher here because of the number of jets involved (16), requiring detailed balance for both the geometry and the mass flow through each of the 32 injecting jets. Establishment of the desired mean stagnation plane requires iteration at all experimental conditions. Slight offsets in the stagnation point locations that remain are smaller than 1 mm in the stagnation-plane region. As an illustration, radial profiles of the normalized mean axial velocity $V/V_{\rm inj}$ are plotted in Fig. 5, at different axial locations. Between the injection point and mid-height ($y/D = 1.53$, for case B), the typical velocity profile corresponds to a (here, confined) counter-flowing mixing layer. The velocity profile is analytically approximated by $V(x, y) \sim \mathrm{erf}(x)\,\mathrm{erf}(y)$ (e.g., Pope (2000). As the stagnation zone is approached, these profiles become increasingly uniform.

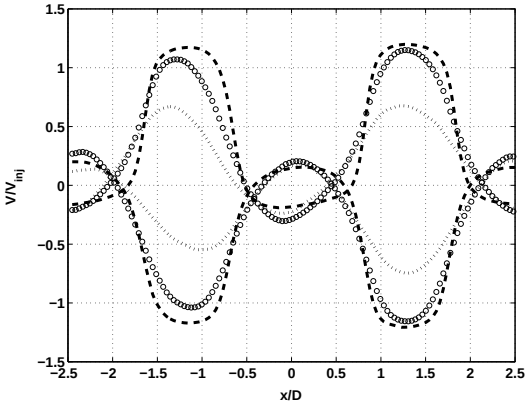


Figure 5: Radial profiles of the normalized mean axial velocity. Dashed line: $y/D = \pm 1.53$; Circles: $y/D = \pm 0.74$; Dotted line: $y/D = \pm 0.26$ (case $B$).

Kostiuk et al. (1993) reported that the uniformity of the vertical flow, in regions where $V(r)$ is nearly uniform, increases as the stagnation zone is approached. They explained this in terms of a higher spatial-spreading rate of the jet in the stagnation region, relative to that observed in free jets. No unusual growth in the $V$-profile is found in the present reactor flows, most-likely because of the confinement effects from the strong recirculation, as further discussed below.

A more-complete picture of the flow emerges from the velocity-field statistics in the mid-span plane, where homogeneity and isotropy are well-respected. Symmetry and periodicity also characterize the flow in this plane. The two types of stagnation points, with zero mean velocity, are also seen in this plane (Fig. 2). The Type-2 stagnation point was discussed in the jet-axis plane description. A third type of stagnation point (Type-3), the central one, occurs between four surrounding pairs of jets. In this region, the flow is also expected to be very nearly axisymmetric.

Another aspect of the mean flow is the mean vorticity field. The interaction between fluid injected at high velocity and the return flow, along with the local-confinement effects,

produce annular mixing layers, as illustrated by the vorticity of the mean flow, $\Omega_Z = \frac{\partial V}{\partial x} - \frac{\partial U}{\partial y}$ (Fig. 6). Regions characterized by non-zero vorticity represent pairs of alternatively rotating coherent rings. These will be identified as 'rings' below and are, basically, annular mixing layers. The high-rotation regions of the flow (rings) have a large effect on the global features of the flow. The ratio of the transport time in the reactor dictated by the mean velocity field and the turbulence characteristic time (defined as the mean kinetic energy divided by the mean energy dissipation rate) is about 1/6, i.e., slow, quasi-frozen turbulence is rapidly transported by the mean velocity field.

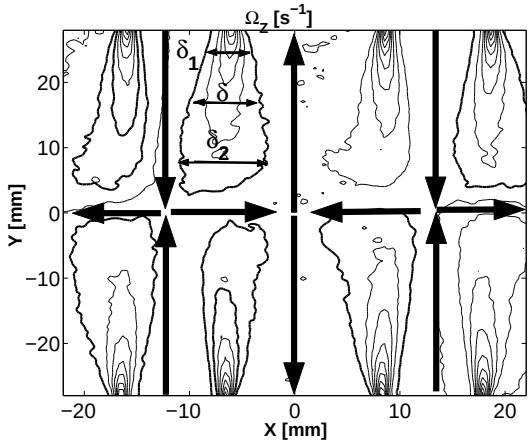


Figure 6: Mean vorticity $\Omega_Z$ distribution in the jet-axis plane. $\delta$ is the width of the rings, or of the annular mixing layers (case $B$), varying between $\delta_1$ (near the injection) and $\delta_2$ (central zone of the reactor).

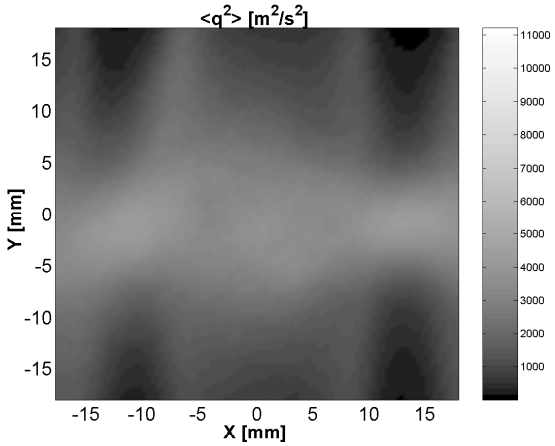


Figure 7: Distribution of the total kinetic energy $\langle u_i u_i \rangle$ in the jet–axis plane.

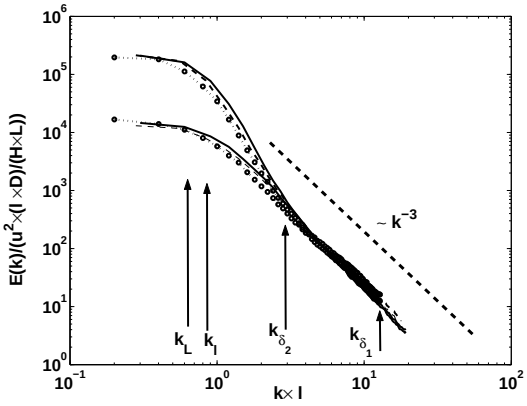


Figure 8: Dimensionless power energy spectra for $u$ (lower curves) and for $v$ (upper curves), in the jet-axis plane, for three cases $A$ (solid line), $B$ (—) and $C$ (dashed line and ∘). The dashed line represents the scaling $\sim k^{-3}$.

## ENERGY SPECTRA

This section discusses the relation of the mean flow to the resulting turbulence and turbulent spectra. The mean velocity field has been decomposed in the regions described above. An understanding of their impact on the turbulent environment is facilitated by an examination of the kinetic energy distribution and of the energy spectra.

Turbulent fluctuations are mainly produced during strong compression of the axial mean velocity, in the stagnation region. Therefore, turbulent kinetic energy (calculated using axisymmetry hypothesis) in concentrated in the central region of the reactor (see Fig. 7), while less energy is present in the injection regions. The central region of the reactor presents properties of local homogeneity.

Figure 8 shows cuts of the two-dimensional energy spectrum calculated over the whole image in the jet-axis plane, as a function of the dimensionless wavenumber $k \times \ell$ ($\ell$ is the scale in the vertical direction, over which the mean vertical velocity decreases to zero).

Noteworthy is that the dimensionless spectra, $\frac{E(k)}{\langle u^2 \rangle \frac{\ell \times D}{H \times L}}$, when expressed as functions of $k \times \ell$, are similar irrespective of injection conditions, suggesting that the similarity scales are $\ell$ and $\langle u_i^2 \rangle$.

The spectra can be decomposed into two regimes. First, the low-wavenumber part contains most of the energy and is associated with the central (stagnation) region of the reactor, where the impingement of each pair of opposed jets introduces significant fluctuating kinetic energy. The characteristic scales in this region are (Fig. 8): the length $\ell$ in the vertical direction, and the horizontal scale $L$, i.e., half the horizontal distance between each consecutive jet.

Second, for intermediate wavenumbers, between $k_{\delta_1}$ and $k_{\delta_2}$, a $k^{-3}$ regime is found for all Reynolds numbers investigated. A $k^{-3}$ regime is characteristic of turbulence in rotation (e.g., Cambon et al. 2004 and Smith & Wallefe 1999). For rotating turbulence, this wavenumber scaling can be attributed to simple dimensional arguments: the only parameters that should play a role are $\Omega$ (the rotation frequency) and the wavenumber $k$. The only possible combination of these leads to $E(k) \sim \Omega^2 k^{-3}$. Flow regions in strong rotation generate flows characterized by quasi-two-dimensional statistics, in a plane perpendicular to the rotation axis (Hossain 1991, 1994).

Secondly, the range of scales corresponding to the $k^{-3}$ regime is traceable to the characteristic dimensions of the axisymmetric mixing layers, $\delta_1$ and $\delta_2$. Such mixing layers, especially in the near-field region, are 'populated' by energetic coherent vortices. These can be visualized using PLIF (Planar Laser Induced Fluorescence) on acetone measurements, as proposed by Picket & Ghandi (2002), for example. Once their diameter and distance between each pair can be identified, the empirical analysis proposed by Huang & Ho (1990) could be applied, leading to a spectrum

slope very close to $-3$. Huang & Ho (1990) showed that the exponent of the power spectra reached the asymptotic $-5/3$ value at a normalized streamwise position $Rx/\lambda \approx 8$, where $R = (1-r)/(1+r)$, $r = U_2/U_1$ is the velocity ratio of the two streams, and $\lambda$ is the wavelength of the initial large-scale structure. Applying this criterion to our flow (Huang & Ho 1990, Figs. 12 and 13) also leads to a spectral slope very close to $-3$. We note, however, that this is an application of the experimental criterion they proposed for free planar mixing layers and may not apply to the confined axisymmetric mixing layers encountered here.

These explanations are not independent since the presence of strong large-scale vortices can lead to flow with properties similar to turbulence in (local) rotation, and so to spectra close to those that emerge from a clean mathematical analysis (Smith & Wallefe 1999). The role of the vortices on turbulence spectra has already been investigated experimentally by e.g., Simand et al. (2000) and Nickels & Marusic (2001), with similar conclusions.

Strong, unstable coherent vortices are present and impose their signature over the turbulent field and spectra. The role played by coherent structures/vortices has been emphasized in different experimental flows, either 2-D or quasi-2-D (Rutgers 1998 and Paret et al. 1999), or fully 3-D (Simand et al. 2000, and Nickels & Marusic 2001). Simand et al. (2000) studied strong-vortex flows in the von Kármán geometry, where a confined flow is generated inside a cylinder, in the gap between two coaxial disks. When the disks rotate at the same speed, the flow is essentially in global rotation, with a strong axial vortex, stable in time. Hot-wire measurements reveal that in the proximity of the vortex, the slope of the energy spectrum strongly deviates from the classical value of $-5/3$ and tends to almost $-3$, that is characteristic of 2-D flows. The slope evolution might be attributed to the evolution of the flow through the 2-D state in this zone of the flow. Rotation has been shown to be responsible for such flow characteristics, e.g., Smith & Wallefe (1999), Cambon et al. (2004), and Morize et al. (2005).

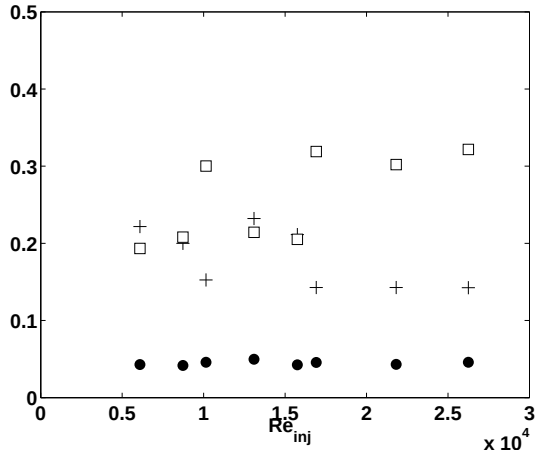


Figure 9: Variation of the ratios $Re_\lambda/Re_{\rm inj}$ ($\bullet$); $u'/V_{\rm inj}$ ($\square$) and $\lambda/D$ ($+$) versus injection Reynolds number.

A comment on Taylor-microscale Reynolds numbers attained in the reactor is in order. Figure 9 represents the dependence of $Re_\lambda/Re_{\rm inj}$, calculated in a point of the outflow where both $u$ and $v$ fluctuations have almost-Gaussian distribution (before fluctuations decay but after the stagnation points where most of the fluctuations are created), as a function of injection Reynolds number. The constant value of this ratio (equal to 0.04), indicating a linear dependence of $Re_\lambda$ on $Re_{\rm inj}$, is interesting.

In classical flows, the root-mean-square velocity fluctuation level scales with the outer-flow velocity, $V_{\rm inj}$ in the present flow, with $u'/V_{\rm inj}$ then expected to be very-nearly independent of the outer-flow Reynolds number, $Re$, where $Re = Re_{\rm inj}$ in our flow (e.g., Jimenez et al. 1993, Dimotakis 2005). This statement is also true in the present flow, as can be seen in Fig. 9.

However, at least in unconfined flows, the Taylor microscale, $\lambda$, typically scales in such a way as to yield $Re_\lambda = u'\lambda/\nu \propto \sqrt{Re}$, where $Re$ is the outer-flow/integral-scale Reynolds number (e.g., Pope 2000, Dimotakis 2005). This is not the case in the present flow, where flow confinement imposes (nearly) $Re$-independent scaling on the Taylor microscale (see Fig. 9), at least over the range of Reynolds numbers investigated. In the experiments reported in this paper, injection Reynolds numbers are in range of $Re_{\rm inj} = 5000$ to 30,000, with Taylor microscale Reynolds numbers in the range of $Re_\lambda = 200$ to 1200.

## CONCLUSIONS

The confined flow in the reactor studied is generated by an array of opposed jets and can be described as forced-box turbulence. Fluid injected through a total of 32 jets, arranged as two sets of 16 opposed pairs, issues from top/bottom boundary porous planes. Reynolds numbers investigated, based on injection velocity and jet diameter, were up to 30,000. The high Reynolds numbers and impinging configuration of the flow produce very intense turbulence levels.

PIV measurements in different planes allowed for a characterization of the mean and fluctuating velocity fields. Fluid recirculation in the reactor creates annular mixing layers, seen as large-scale pairs of alternatively rotating large-scale coherent rings. The large-scale properties of the mean flow, i.e., the large-scale vorticity and strain, leads to quasi-two-dimensional turbulence at the largest scales. The central region of the reactor includes stagnation regions, where mean vertical velocity gradients are very strong with low local mean velocity values, leading to high rms-to-mean velocity ratios. Such gradients are responsible for considerable kinetic-energy production, that sharply peaks in the central region.

An important finding is that the spectra exhibit a well-defined $k^{-3}$ regime, over a relatively wide range of wavenumbers. This may be attributable to the regions with nearly axisymmetric mixing layers between the injecting-jet and flow-exit regions that are constrained by the tight confinement. Coherent vortices born in those regions, for which the wavelength and distance among them were identified from velocity-field data, are likely responsible for the spectra observed that are similar to those encountered in rotating turbulence.

In the classical-cascade scenario, energy is injected at large scales and transferred to ever-smaller eddies in the course of the cascade. In our flow, energy is introduced into the flow at low wavenumbers and contributes to smaller-scale turbulence generated in the opposed-jet stagnation regions, over the scales $\delta$ or $L$. The remainder of Lagrangian time the fluid spends in the interior of the reactor is small in comparison with the cascade time (less than 1/6), so there is insufficient time for the cascade to develop. Such flows are referred to as "frozen", or "baby" turbulence. The mixing layers in the present reactor develop in a confined environ-

ment and are different from free mixing layers. The effects of flow confinement are also responsible for producing Taylor microscale Reynolds numbers, $Re_\lambda$ that are proportional to outer-flow/integral-scale Reynolds numbers, $Re$, in contrast to developing, unconfined flows where $Re_\lambda$ is typically proportional to the square root of the outer-flow Reynolds number. For a given outer-flow Reynolds number, this also produces higher-$Re$ turbulence.

Financial support from the French Minister of Education, under the grant 'Jeunes Chercheurs' No 035181, and from the French National Research Agency (project 'Micromélange' N$^o$ NT05 - 2 42482) is gratefully acknowledged.

## REFERENCES

Birouk, M., Sahr, B., and Gokalp, I., 2003, "An attempt to realize experimental isotropic turbulence at low Reynolds numbers", *Flow, Turb. Comb.*, Vol. 70, pp. 325-348.

Cambon, C., Rubinstein, R. and Godeferd, F., 2004, "Advances in wave turbulence: rapidly rotating flows", *New J. Phys.*, Vol. 6, p. 73.

Dimotakis, P.E., 1991, "Turbulent free shear layer mixing and combustion", *In S.N.B. Murthy and E.T. Curran (Editors), High-Speed flight Propulsion Systems* (Washington, A.I.A.A.), pp. 265–340.

Dimotakis, P.E., 2005, "Turbulent Mixing." *Ann. Rev. Fluid Mech.* Vol. 37, pp. 329–356.

Foucaut, J.M., Carlier, J., and Stanislas, M., 2004, "PIV optimization for the study of turbulent flow using spectral analysis", *Meas. Sci. Technol.*, Vol. 15, pp. 1046–1058.

Hossain, M., 1991, "Inverse energy cascades in three dimensional turbulence", *Phys. Fluids B*, Vol. 3, p. 511.

Hossain, M., 1994, "Reduction of the dimensionality of turbulence due to a strong rotation", *Phys. Fluids*, Vol. 6, p. 1077.

Huang, L.S., and Ho, C.H., 1990, "Small-scale transition in a plane mixing layer", *J. Fluid Mech.*, Vol. 210, p. 475.

Hwang, W., and Eaton, J.K., 2003, "Creating an homogeneous and isotropic turbulence without a mean flow", *Exp. Fluids*, published online.

Jimenez, J., Wray, A.A., Saffman, P.G., and Rogallo, R.S., 1993, "The structure of intense vorticity in homogeneous isotropic turbulence." *J. Fluid Mech.* Vol. 255, pp. 65-90.

Kostiuk, L.W., Bray, K.N.C., and Cheng, R.K., 1993, "Experimental study of premixed turbulent combustion in opposed streams. Part I – Nonreacting flow field.", *Comb. Flame*, Vol. 92, pp. 377–395.

Foucaut, J.M., Carlier, J., and Stanislas, M., 2004, "PIV optimization for the study of turbulent flow using spectral analysis", *Meas. Sci. Technol.* Vol. 15, pp. 1046–1058.

Krawczynski, J.F., Renou, B., Danaila, L., and Demoulin, F.X., 2006a, "Small-scale measurements in a Partially Stirred Reactor (PaSR)", *Exp. Fluids*, Vol. 40, pp. 667–682.

Krawczynski, J.F., Renou, B., Dimotakis, P.E., and Danaila, L., 2006b, "Determination of the kinetic energy dissipation rate in a Partially Stirred Reactor", *13-th International Symposium on applications of Laser Techniques to Fluid Mechanics* (Lisbon, 26-29 June 2006).

Markides, C.N., and Mastorakos, E., 2006, "Measurements of scalar dissipation in a turbulent plume with planar laser-induced fluorescence on acetone", *Chem. Eng. Sci.*, Vol. 61, p. 2835.

Morize, C., Moisy, F., and Rabaud, M., 2005, "Decaying grid-generating turbulence in a rotating tank", *Phys. Fluids*, Vol. 17, p. 095105.

Nickels, T.B., and Marusic, I., 2001, "On the different contributions of coherent structures to the spectra of a turbulent round jet and a turbulent boundary layer", *J. Fluid Mech.*, Vol. 448, p. 367.

Paret, J., Jullien, M.C., and Tabeling, P., 1999, "Vorticity statistics in the two-dimensional enstrophy cascade", *Phys. Rev. Lett.*, Vol. 83, p. 3418.

Pickett, L.M., and Ghandhi, J.B., 2002, "Passive scalar mixing in a planar shear layer with laminar and turbulent inlet conditions", *Phys. Fluids*, Vol. 14, p. 985.

Pope, S.V., 2000, *Turbulent flows*. Cambridge University Press.

Rolon, J.C., Veynante, D., and Martin, J.P., 1991, "Counter jet stagnation flows", *Exp. Fluids*, Vol. 11, pp. 313–324.

Rutgers, M.A., 1998, "Forced 2D turbulence: experimental evidence of simultaneous inverse energy cascade and forward enstrophy cascade", *Phys. Rev. Lett.*, Vol. 81, p. 2244.

Simand, C., Chillà, F., and Pinton, J.F., 2000, "Inhomogeneous turbulence in the vicinity of a large-scale coherent vortex", *Europhys. Lett.*, Vol. 49, p. 336.

Smith, L.M., and Wallefe, F., 1999, "Transfer of energy to two-dimensional large scales in forced, rotating three-dimensional turbulence", *Phys. Fluids*, Vol. 11, 6, pp. 1608–1622.